Phase evolution and critical behavior in strain-tuned $LaMnO_3$-$SrMnO_3$ superlattices

Hiroyuki Yamada,[1] Ping-Hua Xiang,[1,2] and Akihito Sawa[1]
[1]*Nanoelectronics Research Institute (NeRI), National Institute of Advanced Industrial Science and Technology (AIST), Tsukuba, Ibaraki 305-8562, Japan*
[2]*Japan Science and Technology Agency (JST), CREST, Kawaguchi 332-0012, Japan*
(Received 11 August 2009; revised manuscript received 22 October 2009; published 14 January 2010)

Mott insulator superlattices, $LaMnO_3$-$SrMnO_3$, grown on lattice-matched $La_{0.3}Sr_{0.7}Al_{0.65}Ta_{0.35}O_3$ substrates were investigated as to the influence of the thicknesses of $LaMnO_3$ (m unit cells [uc], $2 \leq m \leq 10$) and $SrMnO_3$ (n uc, $2 \leq n \leq 6$) layers on the electronic and magnetic properties. The superlattices exhibited dramatic phase evolution and critical behavior when the structural imperfections were significantly diminished. Ground states of the superlattices were mostly ferromagnetic insulator (nonmetal), whereas typical ferromagnetic metal (FM) could be realized for $m > n$ and $n=2$. For $m=2$, the antiferromagnetic insulator (AFI) was stabilized for $n \geq 3$ and an insulating state persisted even down to $n=2$. Around the metal-insulator boundary, the superlattices exhibited magnetorelaxorlike large magnetoresistance and in the case of $m=n=2$, a magnetic field induced an insulator-metal transition, which is unpredictable from $La_{1-x}Sr_xMnO_3$ bulk and alloy films. Detailed analyses of the magnetic field dependences of magnetization and resistivity for the superlattices indicated that the phase separation of FM and AFI may occur at the interface and the AFI state may change to the FM state by applying a magnetic field.

DOI: 10.1103/PhysRevB.81.014410 PACS number(s): 73.21.Cd, 75.70.Cn, 75.47.Gk, 75.47.Lx

I. INTRODUCTION

The interface-specific metallic phase, created from insulating components, is one of the most exciting topics in the field of oxide electronics since the discoveries of high-mobility electron conduction and even superconductivity at the interface between the band insulators $SrTiO_3$ (STO) and $LaAlO_3$ (LAO).[1] The polar discontinuity between STO and LAO may create a quasi-two-dimensional electron gas at the interface. In the case of strongly correlated transition-metal oxides, recent studies have revealed that a charge transfer induces a metallic phase in superlattices composed of two Mott insulators such as $LaMnO_3$ (LMO) and $SrMnO_3$ (SMO).[2,3] Because the LMO-SMO superlattices show diverse magnetic and electronic phases depending on the superlattice period, the LMO-SMO interface is of considerable interest. Early studies of LMO-SMO superlattices showed that short-period superlattices are ferromagnetic metal (FM), as expected from alloy perovskite manganites, whereas long-period superlattices exhibit ferromagnetism only at the interface.[4] However, recent studies with advanced methods have revealed various aspects in this system. Neutron reflectometry showed that the interfacial magnetic state alters intricately depending on the periodicity and roughness of the interfaces.[3,5] On the other hand, transport characteristics seem to be dominated by the interface.[6] Resonant x-ray scattering suggested a small valence modulation in the LMO and SMO layers.[7] That study also pointed out that the superlattices are mostly insulators and experimentally, their transport and structural properties strongly vary from run to run.

Those nontrivial results imply that complicated ground states at the interface, which are governed by a strong coupling between charge, spin, and orbital degrees of freedom, are very sensitive to the layer thickness or extrinsic disorder. In addition, substrate choice (the epitaxial strain from a substrate) is also crucial to the ground states at the interface. An STO substrate, as adopted in previous studies, has a lattice constant ($a=0.3905$ nm) larger than the averaged values of the constituent LMO and SMO. It has been pointed out that the tensile strain due to STO suppresses the interface ferromagnetism[8] and the lattice matching, realized by an $La_{0.3}Sr_{0.7}Al_{0.65}Ta_{0.35}O_3$ (LSAT, $a=0.3870$ nm) substrate, stabilizes the ferromagnetism in the superlattice.[9,10] Accordingly, in order to fully understand the ground states of the superlattice, it is necessary to investigate systematically the magnetic and transport properties of the superlattice with high precision.

In this paper, we report the ground-state phase diagram of LMO-SMO superlattices grown on LSAT substrates. A set of optimized samples revealed a rich variety of electronic phases, ranging from FM to antiferromagnetic insulator (AFI), or ferromagnetic insulator (FI), depending on the thickness of each layer. An intriguing large magnetoresistance (MR) effect was found in the superlattice at the FM-FI (AFI) phase boundary. Those phenomena, which are unprecedented in superlattices on STO substrates or $La_{1-x}Sr_xMnO_3$ (LSMO) in bulk form or as an alloy film, are discussed in terms of competing FM-AFI ground states at the interface and charge-spin-orbital modulations in the superlattice.

The paper is organized as follows. Section II describes the fabrication and characterization, as well as the impact of optimization on the superlattice properties. Section III A discusses a possible phase diagram of the superlattices evaluated in terms of the influence of the layer thickness on the magnetic and electronic properties. In Sec. III B, the anomalous MR and electronic properties are described together with the magnetic field dependence data, where the role of interface magnetism is discussed. In Sec. III C, the origin of phase evolutions is further discussed from magnetism in the noninterface region and charge transfer between LMO and SMO. Section IV gives a summary.

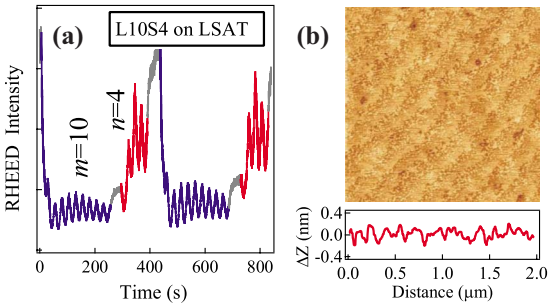

FIG. 1. (Color online) (a) Typical RHEED oscillations during growth of LMO-SMO superlattice grown on LSAT substrate and (b) atomic force microscopy image and line scan of the superlattice showing a step-and-terrace surface. Thicknesses of LMO and SMO layers were 10 uc and 4 uc, respectively, denoted as L10S4.

II. FABRICATION AND CHARACTERIZATION

The superlattices were fabricated on LSAT (001) substrates by pulsed laser deposition. The fabrication has already been reported elsewhere[9] but some conditions were further optimized as described below. Samples were typically grown at 700–720 °C in 3–5 mTorr oxygen pressure. The laser fluence was optimized independently for the LMO and SMO. The resultant samples had smooth surfaces. Figure 1 shows the intensity of a specular spot in reflection high-energy electron diffraction (RHEED) during the growth of the superlattice, where the layer-thickness LMO [m unit cells (uc)] and SMO [n uc] (denoted as LmSn) were set to $(m,n)=(10,4)$ [L10S4]. Due to the precise control of the growth conditions, clear oscillations persisted for such thicker layers. Surface flatness was confirmed with atomic force microscopy [Fig. 1(b)], showing 0.4-nm-high steps originating from misorientation of the substrate. The thickness of the films was around 40 nm. The total repetition for the superstructure was determined to be around $100/(m+n)$.

Their structures were characterized by x-ray diffraction (XRD; Bruker, D8 Discover). The flatness of the film appeared as clear Laue fringes. We also watched out for superlattice reflections because their relative intensities correlate with the regularity of the superlattice period and the flatness of the interfaces. Intensity asymmetry between ± 1 reflections can be interpreted as nonuniform lattice spacing under sharp La/Sr modulation.[7] As typical examples, the XRD spectra of LmSn for $m=n=2$, 4, and 5 are displayed in Figs. 2(a)–2(c), respectively. The superlattice peaks were remarkably sharpened by carefully setting the growth parameters within the above ranges. Here we define a sample showing sharp, asymmetric superlattice reflections as a *good* sample, and a sample showing unclear, symmetric superlattice reflections as a *bad* sample. In fact, the periodicity ($m+n$) of the good ones, evaluated from the superlattice reflections, differed from the designed value by less than 3%, whereas much larger deviations (>5%) were observed in the bad ones.[11]

Resistivity (ρ) and magnetization (M) were measured with a Quantum Design PPMS and MPMS, respectively. The magnetic field was applied parallel to the in-plane [100] direction. The quality of the superlattice in terms of the structural perfection significantly affects both the magnetic and transport properties, especially at shorter periodicity. Figures 2(d)–2(f) show the temperature dependence of M and ρ for the superlattices with $m=n=2$, 4, and 5, respectively. The bad samples had higher Curie temperature (T_C), and below T_C, larger M, and lower ρ than the good ones. This means that the bad samples tended to be FM irrespective of the periodicity. Therefore, the growth-condition-dependent tendency toward FM characteristics could be ascribed to dislocation or interface roughening. The narrow window for the optimal growth is due to the difficult optimization and incompatible growth conditions for LMO and SMO films.[7,12]

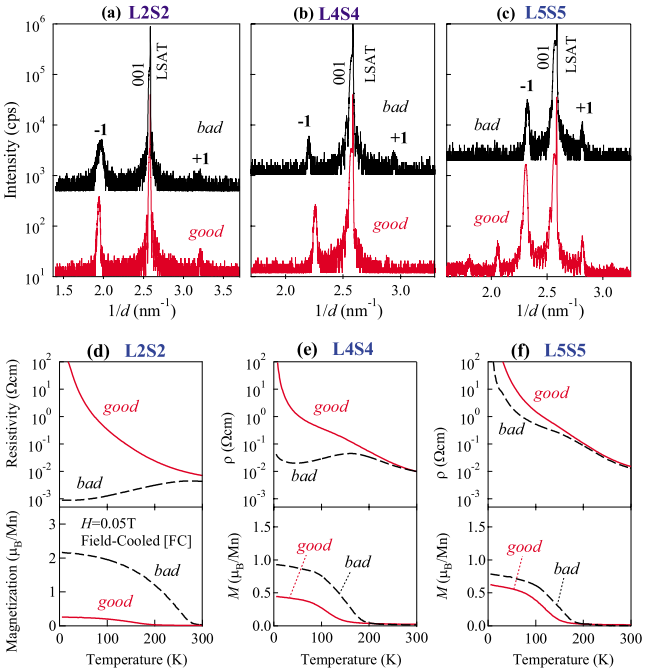

FIG. 2. (Color online) X-ray θ-2θ scan around (001) diffraction for good and typical bad samples of (a) L2S2, (b) L4S4, and (c) L5S5 superlattices grown on LSAT substrates. The 2θ value is converted into the reciprocal of lattice spacing ($1/d$ value). First-order superlattice reflections are denoted as ± 1. Temperature profiles of resistivity (ρ) and magnetization (M) for the good (solid line) and bad (broken line) samples of (d) L2S2, (e) L4S4, and (f) L5S5.

III. RESULTS AND DISCUSSIONS

A. Overview of phase diagram: Temperature dependence

We first discuss the ground states of the short-period LmSn superlattices ($m+n \leq 6$) based on the magnetic and electronic properties of the good samples. Figure 3(a) shows the ρ-temperature (T) and M-T curves of the LmSn superlattices. As seen in Fig. 3(a), even in the short-period superlattices, the magnetic and electronic properties were significantly changed depending on m and n. The noticeable point is that L2S2 is not a metal but an insulator ($\gg 100$ Ω cm at 10 K) with reduced spontaneous M and T_C (200 K). If the charge transfer, i.e., the leakage of Mn-e_g electrons from LMO to SMO, extends over one or more uc from the interface, the valence of Mn ions in L2S2 may average out

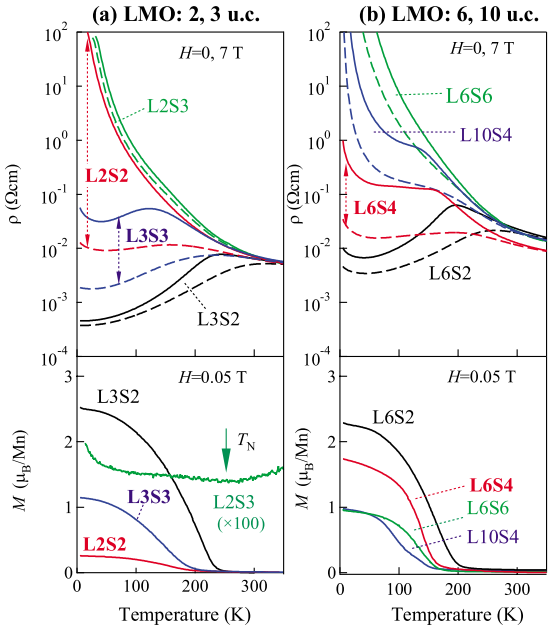

FIG. 3. (Color online) Temperature (T) profiles of resistivity (ρ) and magnetization (M) for the LMO-SMO superlattices with (a) 2 or 3 uc LMO layers and (b) 6 or 10 uc LMO layers. Measurement magnetic fields for ρ-T were 0 and 7 T, shown as solid and broken lines, respectively. For clarity, M for L2S3 is multiplied by 100 and an offset is applied.

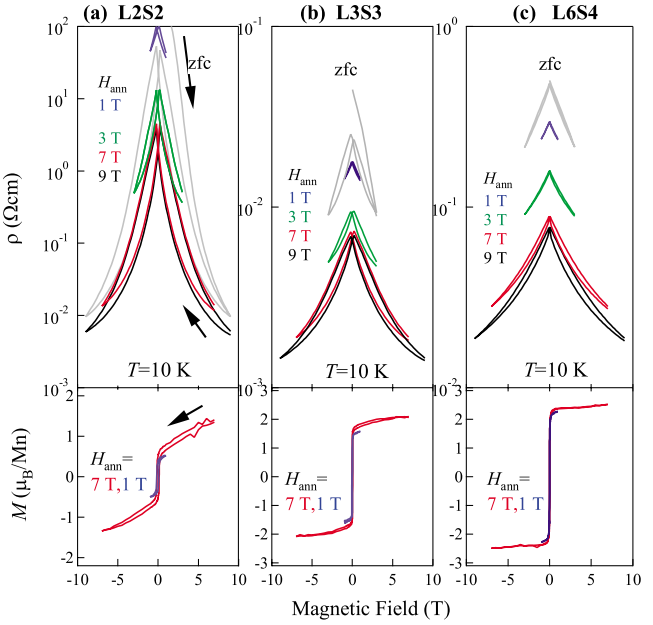

FIG. 4. (Color online) Magnetic field (H) dependence of resistivity (ρ) and magnetization (M) at $T=10$ K for (a) L2S2, (b) L3S3, and (c) L6S4 superlattices, respectively. The ρ-H curve was measured after annealing with various fields H ($H_{ann}=1,3,7,9$ T), or zero-field cooling. The M-H curve was measured for $H_{ann}=1$ and 7 T, which exhibits a slight difference, associated with a large ρ change. The history of H application is indicated by arrows.

around +3.5 throughout the superlattice, where the L2S2 superlattice is expected to behave as an alloy LSMO ($x=0.5$) film. However, although the alloy LSMO ($x=0.5$) film on the LSAT substrate is a ferromagnetic metal,[13] the L2S2 superlattice is an insulator even in the ground state. Therefore, the charge transfer alone cannot explain the properties of the superlattices. Rather, the coupling or competition of various spin and/or orbital states may play a crucial role in the interfacial electronic state. In fact, the L2S2 superlattice showed a large magnetic field response, indicating that a magnetic interaction is involved in the electronic state. The insulator L2S2 turned into a metal in high magnetic field (H). As shown in Fig. 4(a), at the lowest T (10 K), ρ was reduced to as low as 5 m Ω cm ($H=9$ T) and M was increased to $1.3\mu_B$/Mn site ($H=7$ T) but not saturated. It should be noted that the unconventional phenomena in L2S2 cannot be understood from a simple analogy with the properties of the bulk or alloy films (see Appendix).

We also found remarkable layer-thickness dependence. As the SMO layer thickness increased from L2S2, the superlattices became AFI. As seen in Fig. 4(a), L2S3 was AFI with $T_N \sim 250$ K and showed almost no MR effect. We also confirmed that L2S4 was AFI (not shown). The ρ-T and M-T behaviors of these superlattices were similar to those of heavily Sr-doped LSMO (or lightly electron-doped SMO) which shows an orbital-ordered (OO) phase (see Appendix).[14] On the other hand, as the LMO layer thickness increased from L2S2, the superlattices became FM. L3S2 is a conventional FM below $T_C=240$ K.[9,15] Thus, L2S2 is located at the boundary between AFI and FM superlattices. It is well known that in nearly half-doped perovskite manganites, a dramatic phase switching brought about by various external stimuli originates from the competition between FM and orbital/charge-ordered states.[16] From this fact, we can deduce that the observed large MR in L2S2 may be due to the phase competition between AFI and FM. This prediction seems to be supported by the result that L3S3, which is located in the vicinity of AFI-FM boundary, also showed a large MR, although the conductivity below $T<T_C=200$ K was higher than that of L2S2.

We then focused on longer-period ($m+n \geq 8$) superlattices. The symmetric superlattices L4S4 [Fig. 2(e)], L5S5 [Fig. 2(f)], and L6S6 [Fig. 3(b)] behaved as FI with low $T_C=160$ K. They no longer became metallic even at $H=7$ T (only L6S6 is shown). Conducting phases appeared in asymmetric ones: the L6Sn superlattices were nearly FM and FM for $n=4$ and 2, respectively. The L6S4 superlattice became metallic by applying H, where $\rho(0\ \mathrm{T})/\rho(7\ \mathrm{T}) \sim 30$ at 5 K. On the other hand, L10S4 was FI even under magnetic fields, indicating that thicker LMO is unfavorable for FM.

The ρ-H and M-H curves of the superlattices showing a large MR are presented in Fig. 4 and some typical M-H curves of the ferromagnetic superlattices and the alloy LSMO ($x=0.4$) film are shown in Fig. 5(a). The saturation M, or M at 7 T, of the superlattices was smaller than that of the ferromagnetic alloy film, indicating that even in the short-period superlattices, ferromagnetism did not appear over the entire superlattice but only in part of the superlattice. The details will be discussed later on.

On the basis of the above results, a possible phase diagram in Fig. 6(a) summarizes the ground states of LmSn

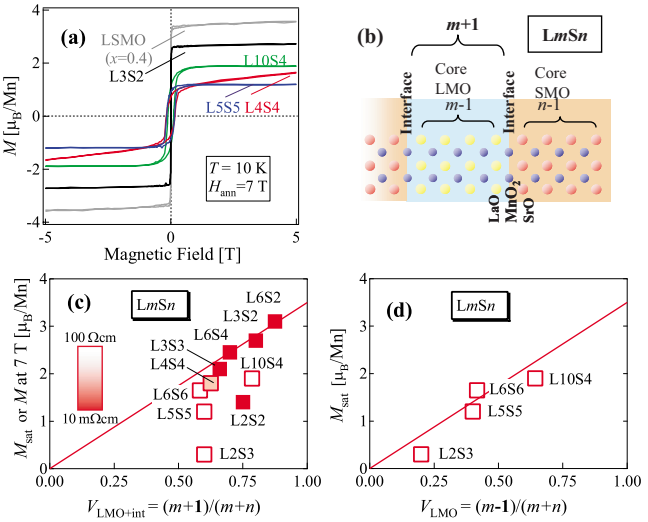

FIG. 5. (Color online) (a) M-H curves at $T=10$ K for typical ferromagnetic LMO-SMO superlattices and alloy LSMO ($x=0.4$) film. (b) Schematic illustration of atomic arrangement of LmSn superlattice composed of $(m-1)$ uc-core LMO, two interfaces and $(n-1)$ uc-core SMO layers in one periodicity $[(m+n)$ uc]. (c) Saturation M (M_{sat}), or M at $H=7$ T, at $T=10$ K for the superlattices plotted against the volume fraction of core LMO and interface layers ($V_{LMO+int}$), which is given by $(m+1)/(m+n)$ in LmSn. Colors in the squares represent the resistivities at $H=7$ T and $T=10$ K, as shown in the scale bar. (d) Saturation M (M_{sat}), or M at $H=7$ T, at $T=10$ K for the insulating superlattices plotted against the volume fraction of the core LMO layer (V_{LMO}), which is given by $(m-1)/(m+n)$.

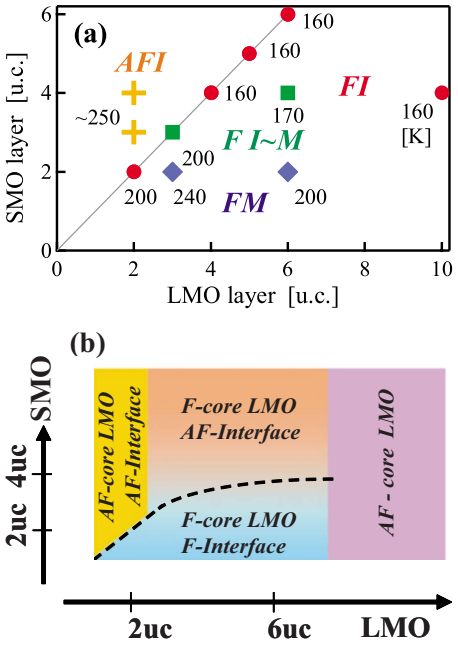

FIG. 6. (Color online) (a) Phase diagram for the LmSn superlattices ($2\leq m\leq 10$ [uc], $2\leq n\leq 6$ [uc]). Ferromagnetic metal, ferromagnetic insulator, and antiferromagnetic insulator are denoted as FM (diamonds), FI (circles), and AFI (crosses), respectively. Nearly FM is denoted as FI~M (squares), where resistivities at T_C and 10 K are on the same order. The numbers in the figure represent T_C or T_N. (b) Local magnetism at the interface and core LMO layers, as a function of layer thicknesses. Ferromagnetic and antiferromagnetic states are denoted as F and AF, respectively.

superlattices as a function of layer thicknesses $(m,n\geq 2)$. They are classified into AFI, FM, nearly FM, and FI phases (more precisely, L2S2 and L4S4 are canted AFI). The clear FM state was observed only for $n=2$ and $m>n$, represented by L3S2 and L6S2. The AFI phase appeared for $m=2$ and $n>m$. The FI phase widely appeared in thicker regimes. Figure 6(a) also gives the T_C value for each sample, determined from the M-T curves.

B. Role of interfaces: Magnetic field dependence

The superlattices in the vicinity of the FM-AFI (FI) boundary, i.e., L2S2, L3S3, and L6S4, exhibited an H-induced insulator (or nearly metal)-to-metal transition. We can extract common features in the MR effect from the H dependences of ρ and M at $T=10$ K (Fig. 4). For all three cases, when the sample was cooled down from $T>T_C$ in the magnetic field (H_{ann}), the H_{ann}-dependent MR effect emerged. Moreover, this H_{ann}-dependent MR was accompanied by enhanced saturation M. This so-called magnetorelaxor behavior is represented by impurity-doped charge/orbital-ordered perovskite manganites, where the FM domain and AFI region (short-range charge/orbital ordering) coexist, that is to say, are phase separated.[17,18] The volume ratio of FM was controlled with H_{ann}. Therefore, the large MR in these superlattices indicates the coexistence and competition between AFI (OO) and FM states.

It should be noted that such a huge, magnetorelaxorlike MR has never been reported in LmSn superlattices grown on STO. This suggests that the lattice matching (epitaxial strain) has a crucial role in the competing magnetic states. In perovskite manganite films, the epitaxial strain controls the spin ordering through the modification of the Mn-e_g orbital ordering.[13] Therefore, the Mn-e_g orbital state may be deeply involved in the magnetic states realized in superlattices on LSAT substrates.

As mentioned in Sec. III A, ferromagnetism appeared in part of the superlattice. To find out which Mn sites contributed to the ferromagnetism, we evaluated the saturation $M(M_{sat})$ of the superlattices at $T=10$ K. In the L2S2 and L4S4 cases, M at $H=7$ T was substituted for M_{sat} because M was not saturated at $H=7$ T (the maximum H value of MPMS). It has been established that optimally doped ferromagnetic LSMO has M_{sat} as large as $3.5\mu_B$/Mn (this value is denoted as M_{LSMO}). In L3S2, representing an FM superlattice, M_{sat} was about $2.7\mu_B$, as seen in Fig. 5(a). This value corresponds to about 80% of M_{LSMO}, where the fraction seems to coincide with the volume fraction of core (non-interfacial) LMO and interface layers ($V_{LMO+int}$). As shown in Fig. 5(b), the basic element of LmSn consists of $(m-1)$ uc-core LMO, $(n-1)$ uc-core SMO, and two interface layers. Thus, $V_{LMO+int}$ is given by $(m+1)/(m+n)$. In Fig. 5(c), M_{sat} (or M at 7 T) at $T=10$ K for the superlattices is plotted against $V_{LMO+int}$. The line in Fig. 5(c) is $M_{sat}=M_{LSMO}\times V_{LMO+int}$ and the colors of the squares indi-

cate the resistivity of the superlattices at $T=10$ K in $H=7$ T. We found that M_{sat} was close to $M_{LSMO}\times V_{LMO+int}$ for the conducting superlattices under $H=7$ T, except for L2S2. This indicates that in the conducting superlattices, the Mn sites adjacent to rock-salt LaO layers are responsible for the ferromagnetism, whereas the core SMO layer is AFI with much smaller M. On the other hand, M_{sat} was smaller than $M_{LSMO}\times V_{LMO+int}$ for the insulating superlattices, even in $H=7$ T. As shown in Fig. 5(d), for some of the FI superlattices (L5S5 and L6S6), M_{sat} seems to be close to $M_{LSMO}\times V_{LMO}$, where V_{LMO} is the volume fraction of the core LMO layer and is given by $(m-1)/(m+n)$. This result implies that in the FI superlattices, only the core LMO layers contribute to ferromagnetism.

The above analyses provide two insights into the electronic and magnetic properties of the superlattices: (1) in the conducting superlattices, including those showing the magnetorelaxorlike MR, the interfaces, and core LMO layers contribute to ferromagnetism and (2) in the insulating superlattices, only core LMO layers contribute to ferromagnetism. From these insights, we can predict that the electronic states of the interfaces dominate the transport properties of the superlattice and the magnetorelaxorlike MR is attributed to the magnetic field-induced AFI-to-FM transition at the interfaces. To verify this, we evaluated the H_{ann}-dependent ρ-H and M-H characteristics of L2S2, L3S3, and L6S4 in detail.

In a typical bulk magnetorelaxor, Cr-doped $Nd_{0.5}Ca_{0.5}MnO_3$ (Cr:NCMO),[17] M_{sat} is about $4\mu_B$/Mn at $H_{ann}=7$ T, and for $H_{ann}<7$ T, M_{sat} is roughly proportional to H_{ann}. Therefore, the volume of the FM region is more or less linearly tunable with $H_{ann}(\leq 7$ T) from $\sim 10\%$ to $\sim 100\%$. As a result of the FM volume increase, resistivity decreases dramatically with low $H_{ann}(<5$ T) and gradually decreases for higher H_{ann}. The former case can be understood as the formation of a percolative conduction path. For the LmSn superlattice case, the H_{ann} dependence on M_{sat} is different from that for bulk Cr:NCMO. As seen in Fig. 4, the LmSn already has a larger M_{sat} even for $H_{ann}=1$ T. Particularly, in the L6S4 superlattice, M_{sat} values for $H_{ann}=7$ and 1 T were 2.4 and $2.3\mu_B$/Mn, respectively, which means that the volume of the ferromagnetic region could be slightly tuned from about 65% to 70%. In spite of the small magnetic change, ρ exhibited sharp H_{ann} dependence for $1\ \text{T}\leq H_{ann}\leq 7$ T. Therefore, in contrast to bulk Cr:NCMO, where AFI (OO) and FM coexist over the entire crystal, the phase separation in this superlattice may occur in limited layers, which can be assigned to interfaces. As discussed above, the interface magnetic state can alter from a ferromagnetic to antiferromagnetic one depending on the layer thicknesses, whereas the spin states in the core LMO and SMO layers remain unchanged. Therefore, it is reasonable to conclude that the phase separation occurs only at the interface and the AFI region at the interface becomes the FM one by applying a magnetic field.

The origin of the interface phase separation is an open question but here we note that A-site ordered perovskite $LaBaMn_2O_6$ bulk exhibits intrinsic phase separation of FM and CE-type charge/orbital ordered AFI.[19] This intriguing property is attributed to the noncentrosymmetric environment of the MnO_2 sublattice sandwiched by LaO and BaO layers. Therefore, in LmSn superlattices, the atomic arrangement of LaO-MnO_2-SrO may also affect the interfacial electronic state, which means that the interfacial layer cannot be simply regarded as LSMO ($x=0.5$) alloy.

C. Origin of anomalous phase evolutions

As discussed in Sec. III B, the LmSn superlattice consists of three distinct parts, i.e., the core LMO, the SMO, and the interface layers, all of which have different electronic and magnetic properties. The spatially varied properties may comprise the ground-state phase diagram of the superlattices, as shown in Fig. 6(a). Therefore, in order to better understand the ground states of the superlattices, it is necessary to distinguish the contribution of each part. Concerning the core SMO layers in the LmSn superlattices, the AFI ground state is stabilized irrespective of m and n ($2\leq m\leq 10$, $2\leq n\leq 6$), as discussed in Sec. III B. On the other hand, the core LMO layer and the interface exhibit altered properties depending on m and n.

On the basis of the analyses of the M-H characteristics, Fig. 6(b) summarizes possible magnetic states in the core LMO layer and the LMO-SMO interface. The core LMO layer is ferromagnetic in most of the LmSn superlattices, except the ones with $m=2$ and $n\geq 3$, and seems to be insulating for all the superlattices presented in this work. It is considered that the charge donation is the main cause of the local electronic states. Since the FI phase appears for $0.1<x<0.2$ in bulk LSMO,[20] the Mn valence in the core LMO layer is naively expected to be about 3.1+ and at most 3.2+. According to the study on resonant x-ray scattering of LmSn superlattices with $m=n\geq 8$,[7] the Mn valences of the core LMO and SMO layers remain 3+ and 4+, respectively, and an intermediate valence is realized only at the interface, which indicates a tiny amount of charge carrier transferred across the LMO-SMO interface. Nanda and Satpathy[21] have theoretically predicted that the charge transfer is restricted to two layers at the interface for LmSn superlattices with $m=2n$ and $n\geq 3$. In the light of those previous works, we consider that, for $m\leq 6$, the Mn valence is slightly larger than 3+ in the core LMO layer, even at the MnO_2 layer adjacent to the interface and this lightly hole-doped state is responsible for the FI character in the core LMO layer. In the case of a thicker LMO layer ($m>6$), the MnO_2 layers around the center of the core LMO layer may behave as bulk LMO, namely, canted AFI. This means that the local ground states at the center are different from those adjacent to the interface, although both Mn sites belong to a common core LMO layer. This spatial variation inside the core LMO layer appears as the two-step transitions observed in the M-T curve of the L10S4 superlattice [Fig. 3(b)]. On the other hand, for the thinner case, namely, $m=2$ and $n\geq 3$ in LmSn, the core LMO layer is AFI, which cannot be explained by the charge transfer. This nontrivial AFI state may be responsible for the unexpected insulating ground state in the L2S2 superlattice, although the origin is not clearly understood in the present study.

At the interface, the FM ground state was seen for $m\geq 3$ and $n=2$, and the AFI state emerged for the region of

other thickness, as shown in Fig. 6(b). As discussed in Sec. III B, the magnetorelaxorlike behavior at the interface suggests that not only the charge transfer but also the competition of spin and/or orbital orderings govern the electronic and magnetic properties at the interface. Further studies on spin and orbital orderings created in the superlattices will provide insights into the spatially varied electronic states, as well as the complicated ground-state phase diagram.

IV. SUMMARY

We studied the ground-state phase diagram of LMO-SMO superlattices on LSAT substrates for various LMO and SMO layer thicknesses. One of the important findings in the current study is that the extrinsic FM character could be diminished by improving the flatness and regularity of the superlattice interfaces. As a result, the improved LMO-SMO superlattices showed layer-thickness-dependent evolutions of FM, AFI, and FI phases. The superlattices in the vicinity of the FM-AFI (or FI) boundary showed critical behavior appearing as magnetorelaxorlike MR, which may originate from the phase competition at the interface. From detailed analyses of the M-H and ρ-H characteristics, the electronic states at the interfacial MnO_2 layers were found to be significantly different from those at the adjacent MnO_2 layers belonging to the LMO and SMO layers. The present study indicates that, in addition to the charge transfer, a coupling or competition of spin, as well as orbital orderings, plays a crucial role in determining the interfacial electronic states of the strongly correlated electron superlattice.

ACKNOWLEDGMENTS

This study was partly supported by MEXT KAKENHI (Grant No. 21750198) and the Mitsubishi Foundation. The authors are grateful to H. Nakao for stimulating this work and enlightening discussions.

APPENDIX

In this section, we present magnetic and transport properties of heavily Sr-doped LSMO ($0.5 \leq x \leq 0.9$) films grown on LSAT substrates in order to compare the electronic states at the LmSn superlattices with those in the alloy films. The ρ-T and M-T curves for the LSMO films are shown in Fig. 7. We confirmed that the Sr (x) dependence of the electronic phase in the LSMO film resembled that in bulk,[14] as described below.

The typical FM ground state was maintained for $x \leq 0.5$. In LSMO ($x=0.55$), the FM transition occurred at $T=260$ K. At $T=150$ K, M decreased, whereas ρ and M were T independent below this temperature. This 150 K anomaly is attributed to the transition to A-type antiferromagnetic metal (AFM) in association with $d(x^2-y^2)$-OO, as reported in bulk LSMO ($x \sim 0.55$).[14] However, unlike bulk crystal, the spontaneous M of the LSMO ($x=0.55$) film did not vanish in the AFM phase. This discrepancy indicates that spin and orbital are not perfectly ordered in the film, presumably because the substrate, which clamps the film, disrupts the change in lattice parameters of the film at the orbital order-disorder transition. Spontaneous M vanished for the LSMO ($x=0.60$) film, where ρ-T was nearly metallic. For $x \geq 0.67$, the ground state of the LSMO film eventually became AFI.

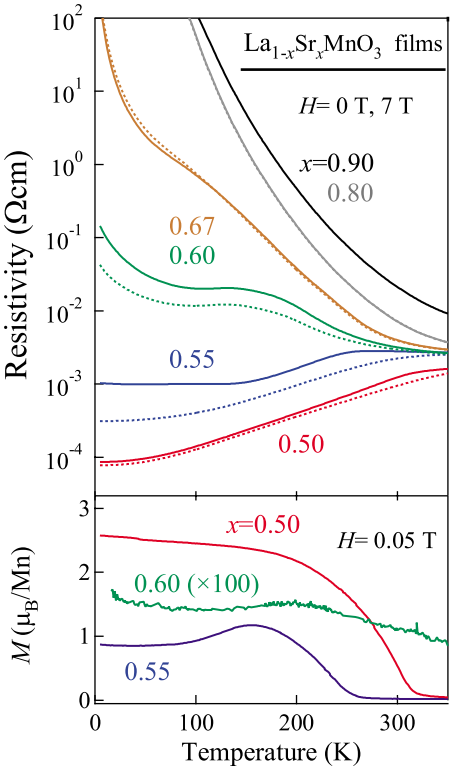

FIG. 7. (Color online) Temperature profiles of resistivity (ρ) and magnetization (M) for alloy LSMO (Sr $x=0.50, 0.55, 0.60, 0.67, 0.80, 0.90$) films grown on LSAT substrates. The ρ-T curve was measured at 0 and 7 T, confirming the absence of colossal MR in the alloy films. The M-T curve was measured at 0.05 T. M for $x=0.60$ film is so small that it is multiplied by 100 for clarity. M for $x \geq 0.67$ (not shown) is as small as that of $x=0.60$.

Importantly, colossal MR [$\rho(0\ \mathrm{T})/\rho(7\ \mathrm{T}) > 10$], as seen in the L$mSn$ superlattice, could not be seen for any x in the LSMO films, even at the metal-insulator boundary regime. On the other hand, the AFM-like behavior as seen in the LSMO ($x=0.55, 0.60$) films was not realized in the LmSn superlattice for $m, n \geq 2$. Therefore, this suggests that the phase evolution in the LmSn superlattice is essentially different from that in LSMO bulk or alloy film.

[1] A. Ohtomo and H. Y. Hwang, Nature (London) **427**, 423 (2004); N. Reyren, S. Thiel, A. D. Caviglia, L. F. Kourkoutis, G. Hammerl, C. Richter, C. W. Schneider, T. Kopp, A.-S. Rüetschi, D. Jaccard, M. Gabay, D. A. Muller, J.-M. Triscone, and J. Mannhart, Science **317**, 1196 (2007).

[2] I. González, S. Okamoto, S. Yunoki, A. Moreo, and E. Dagotto, J. Phys.: Condens. Matter **20**, 264002 (2008) ; S. Dong, R. Yu, S. Yunoki, G. Alvarez, J.-M. Liu, and E. Dagotto, Phys. Rev. B **78**, 201102(R) (2008); S. Smadici, P. Abbamonte, A. Bhattacharya, X. Zhai, B. Jiang, A. Rusydi, J. N. Eckstein, S. D. Bader, and J.-M. Zuo, Phys. Rev. Lett. **99**, 196404 (2007).

[3] A. Bhattacharya, S. J. May, S. G. E. te Velthuis, M. Warusawithana, X. Zhai, B. Jiang, J.-M. Zuo, M. R. Fitzsimmons, S. D. Bader, and J. N. Eckstein, Phys. Rev. Lett. **100**, 257203 (2008).

[4] T. Koida, M. Lippmaa, T. Fukumura, K. Itaka, Y. Matsumoto, M. Kawasaki, and H. Koinuma, Phys. Rev. B **66**, 144418 (2002); P. A. Salvador, A.-M. Haghiri-Gosnet, B. Mercey, M. Hervieu, and B. Raveau, Appl. Phys. Lett. **75**, 2638 (1999).

[5] S. J. May, A. B. Shah, S. G. E. teVelthuis, M. R. Fitzsimmons, J. M. Zuo, X. Zhai, J. N. Eckstein, S. D. Bader, and A. Bhattacharya, Phys. Rev. B **77**, 174409 (2008).

[6] C. Adamo, X. Ke, P. Schiffer, A. Soukiassian, M. Warusawithana, L. Maritato, and D. G. Schlom, Appl. Phys. Lett. **92**, 112508 (2008).

[7] H. Nakao, J. Nishimura, Y. Murakami, A. Ohtomo, T. Fukumura, M. Kawasaki, T. Koida, Y. Wakabayashi, and H. Sawa, J. Phys. Soc. Jpn. **78**, 024602 (2009).

[8] H. Yamada, Y. Ogawa, Y. Ishii, H. Sato, H. Akoh, M. Kawasaki, and Y. Tokura, Science **305**, 646 (2004).

[9] H. Yamada, M. Kawasaki, T. Lottermoser, T. Arima, and Y. Tokura, Appl. Phys. Lett. **89**, 052506 (2006).

[10] B. R. K. Nanda and S. Satpathy, Phys. Rev. B **78**, 054427 (2008).

[11] Our preliminary synchrotron x-ray diffraction experiments confirmed that "good" L2S2 has an extremely regular superlattice structure, whereas "bad" L2S2 includes interface roughness of ~1 uc.

[12] B. Mercey, P. A. Salvador, W. Prellier, T.-D. Doan, J. Wolfman, J.-F. Hamet, M. Hervieu, and B. Raveau, J. Mater. Chem. **9**, 233 (1999).

[13] Y. Konishi, Z. Fang, M. Izumi, T. Manako, M. Kasai, H. Kuwahara, M. Kawasaki, K. Terakura, and Y. Tokura, J. Phys. Soc. Jpn. **68**, 3790 (1999).

[14] Y. Moritomo, T. Akimoto, A. Nakamura, K. Ohoyama, and M. Ohashi, Phys. Rev. B **58**, 5544 (1998); O. Chmaissem, B. Dabrowski, S. Kolesnik, J. Mais, J. D. Jorgensen, and S. Short, *ibid.* **67**, 094431 (2003); J. Hemberger, A. Krimmel, T. Kurz, H.-A. Krug von Nidda, V. Yu. Ivanov, A. A. Mukhin, A. M. Balbashov, and A. Loidl, *ibid.* **66**, 094410 (2002).

[15] T_C values of L3S2 and L6S4 in this study are lower than those in Ref. 9, as a result of further optimization as described in Sec. II.

[16] Y. Tomioka and Y. Tokura, Phys. Rev. B **70**, 014432 (2004); Y. Tomioka, Y. Okimoto, J. H. Jung, R. Kumai, and Y. Tokura, *ibid.* **68**, 094417 (2003).

[17] T. Kimura, Y. Tomioka, R. Kumai, Y. Okimoto, and Y. Tokura, Phys. Rev. Lett. **83**, 3940 (1999).

[18] Y. Ogimoto, M. Izumi, T. Manako, T. Kimura, Y. Tomioka, M. Kawasaki, and Y. Tokura, Appl. Phys. Lett. **78**, 3505 (2001).

[19] T. Nakajima, H. Kageyama, H. Yoshizawa, K. Ohoyama, and Y. Ueda, J. Phys. Soc. Jpn. **72**, 3237 (2003).

[20] A. Urushibara, Y. Moritomo, T. Arima, A. Asamitsu, G. Kido, and Y. Tokura, Phys. Rev. B **51**, 14103 (1995).

[21] B. R. K. Nanda and S. Satpathy, Phys. Rev. B **79**, 054428 (2009).